ISO spectroscopy of shocked gas in the vicinity of T Tau

van den Ancker, M.E.; Wesselius, P.R.; Tielens, A.G.G.M.; Dishoeck, E.F.; Spinoglio, L.

Publication date
1999

Published in
Astronomy & Astrophysics

Astron. Astrophys. 348, 877–887 (1999)

ASTRONOMY AND ASTROPHYSICS

ISO spectroscopy of shocked gas in the vicinity of T Tauri⋆

M.E. van den Ancker[1], P.R. Wesselius[2], A.G.G.M. Tielens[2,3,4], E.F. van Dishoeck[5], and L. Spinoglio[6]

[1] Astronomical Institute "Anton Pannekoek", University of Amsterdam, Kruislaan 403, 1098 SJ Amsterdam, The Netherlands
[2] SRON, P.O. Box 800, 9700 AV Groningen, The Netherlands
[3] Kapteyn Astronomical Institute, Groningen University, P.O. Box 800, 9700 AV Groningen, The Netherlands
[4] NASA Ames Research Center, MS 245-3, Moffett Field, CA 94035, USA
[5] Leiden Observatory, P.O. Box 9513, 2300 RA Leiden, The Netherlands
[6] CNR-Istituto di Fisica dello Spazio Interplanetario, Area di Ricerca Tor Vergata, Via Fosso del Cavaliere, I-00133 Roma, Italy

Received 26 May 1999 / Accepted 28 June 1999

Abstract. We present the results of ISO SWS and LWS spectroscopy of the young binary system T Tau. The spectrum shows absorption features due to H_2O ice, CO_2 ice, gas-phase CO and amorphous silicate dust, which we attribute to the envelope of T Tau S. We derive an extinction of $A_V = 17\overset{\mathrm{m}}{.}4 \pm 0\overset{\mathrm{m}}{.}6$ towards this source. Detected emission lines from H I arise in the same region which is also responsible for the optical H I lines of T Tau N. These lines most likely arise in a partially ionized wind. Emission from the infrared fine-structure transitions of [S I], [Ar II], [Ne II], [Fe II], [Si II], [O I] and [C II] was also detected, which we explain as arising in a ≈ 100 km s^{-1} dissociative shock in a fairly dense (5×10^4 cm^{-3}) medium. Pure rotational and rovibrational emission from molecular hydrogen was detected as well. We show the H_2 emission lines to be due to two thermal components, of 440 and 1500 K respectively, which we attribute to emission from the dissociative shock also responsible for the atomic fine-structure lines and a much slower (≈ 35 km s^{-1}) non-dissociative shock. The 1500 K component shows clear evidence for fluorescent UV excitation. Additionally, we found indications for the presence of a deeply embedded ($A_V > 40^{\mathrm{m}}$) source of warm H_2 emission. We suggest that this component might be due to a shock, caused by either the outflow from T Tau S or by the infall of matter on the circumstellar disk of T Tau S.

Key words: stars: circumstellar matter – stars: individual: T Tau – stars: pre-main sequence – ISM: jets and outflows – infrared: stars

1. Introduction

T Tauri (HD 284419) might well be the most studied young stellar object in the sky. It was initially thought of as the prototype of a class of low-mass pre-main sequence stars, but is now known to be a very unique young binary system. An infrared companion, T Tau S, was discovered $0\overset{''}{.}7$ south of the optically bright K0–1e T Tauri star T Tau N (Dyck et al. 1982), corresponding to a projected separation of 100 AU at the 140 pc distance of the Taurus-Auriga complex (Kenyon et al. 1994; Wichmann et al. 1998). Reports of a third stellar component in the T Tau system (Nisenson et al. 1985; Maihara & Kataza 1991) remain unconfirmed (Gorham et al. 1992; Stapelfeldt et al. 1998). Whereas T Tau N dominates in the optical and at submm wavelengths, the brightness of the system in the infrared is dominated by T Tau S (Hogerheijde et al. 1997). Both T Tau N and S display irregular photometric variability, possibly connected to variations in the rate of accretion of material onto the stellar surface (Herbst et al. 1986; Ghez et al. 1991). Recent HST imaging failed to detect T Tau S in the V band down to a limiting magnitude of $19\overset{\mathrm{m}}{.}6$, showing that $A_V > 7^{\mathrm{m}}$ towards this source (Stapelfeldt et al. 1998). T Tau N, on the other hand, only suffers little extinction ($A_V = 1\overset{\mathrm{m}}{.}39$; Kenyon & Hartmann 1995). Proper-motion studies (Ghez et al. 1995) as well as the discovery of a bridge of radio emission connecting both components (Schwartz et al. 1986) prove beyond doubt that both stars are physically connected, demonstrating that a significant amount of dust must be present within the binary system itself.

In the last few years, millimeter interferometry has revealed the presence of a circumstellar disk with a total mass of 10^{-2} M$_\odot$ around the optically bright component T Tau N. The presence of a cicumstellar disk around T Tau S is suggested by mid-infrared emission, but the millimeter interferometric data show that its mass is substantially less than that around T Tau N (Hogerheijde et al. 1997; Akeson et al. 1998). Lunar occultation observations of the T Tau system show that these disks must be smaller than 1 AU at 2.2 μm (Simon et al. 1996). In addition to this, an envelope or circumbinary disk of similar mass as the T Tau N disk is required to fit the energy distribution and polarization properties of the system (Weintraub et al. 1992; Whitney & Hartmann 1993; Calvet et al. 1994; Hogerheijde et al. 1997). On larger spatial scales, two nebulae are associated with the T Tau system. A small ($\approx 10\,''$) cloud, Burnham's nebula (HH 255), is centered on the binary and shows a line spectrum typical of Herbig-Haro

Send offprint requests to: M.E. van den Ancker (mario@astro.uva.nl)

⋆ Based on observations with ISO, an ESA project with instruments funded by ESA Member States (especially the PI countries: France, Germany, the Netherlands and the United Kingdom) and with the participation of ISAS and NASA.

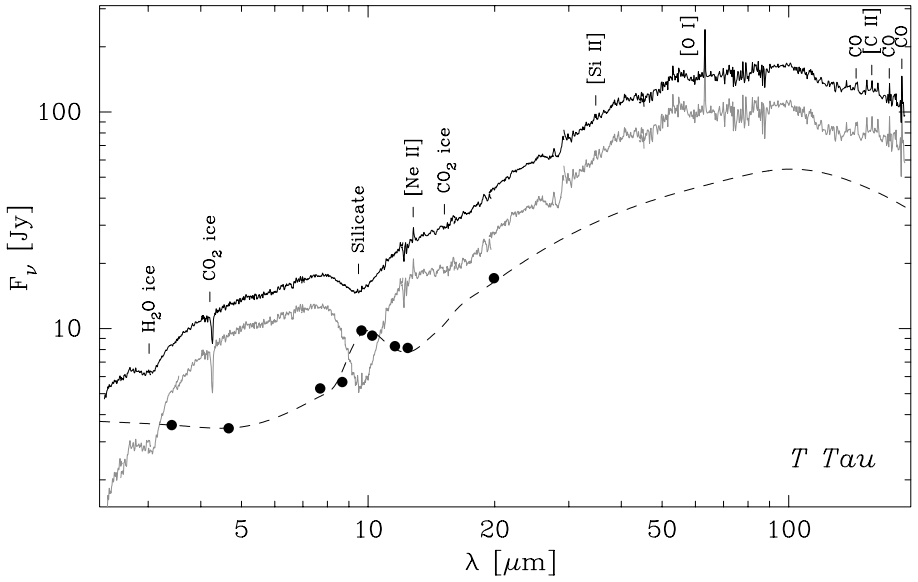

Fig. 1. Combined SWS/LWS full grating spectra for T Tau with the most prominent features identified. The apparent dips at 12 and 28 μm as well as the bump around 52 μm are artefacts of the data reduction process. Also shown (dots) is ground-based photometry of T Tau N with a dust shell model fit to these points (dashed line). The grey curve shows the model-subtracted ISO spectra.

objects (Robberto et al. 1995). A spatially separated arc shaped cloud, Hind's nebula (NGC 1555) is located 30″ to the west. Recent maps at 450 and 850 μm have detected a Class I protostar in Hind's nebula, suggesting that star formation in the vicinity of T Tau is more active than previously thought (Weintraub et al. 1999).

The kinematics of molecular material in the vicinity of T Tau have been found to be very complex. Submm observations of CO and HCO^+ (Knapp et al. 1977; Edwards & Snell 1982; Levreault 1988; van Langevelde et al. 1994a; Momose et al. 1996; Schuster et al. 1997; Hogerheijde et al. 1998) suggest that both components of T Tau drive separate bipolar outflows and that at least one of these is directed close to the line of sight. On even larger scales, Reipurth et al. (1997) discovered a giant Herbig-Haro flow (HH 355) with a projected extent of 38 arcminutes (1.55 pc at 140 pc), aligned with the axis of the outflow from T Tau S, which they explained as being due to multiple eruptions of material while the flow axis is precessing. Ray et al. (1997) showed that T Tau S has recently ejected two large lobes of mildly relativistic particles, demonstrating that the emergent picture might be further complicated by significant time-variability in the outflow rate.

In this paper we present new *Infrared Space Observatory* (ISO; Kessler et al. 1996) spectroscopy of the T Tau system. In Sects. 3 and 4 we analyze solid-state and gas-phase absorption features and show that these are fairly typical for the envelope of an embedded low-mass young stellar object. In Sect. 5 we briefly discuss the infrared H I lines and argue that these have the same origin as the optical lines. In Sects. 6 and 7 we will discuss the observed H_2 spectrum and the atomic fine-structure lines, and show that these are due to shocked gas. In the discussion (Sect. 8) we will argue that the most likely candidate for a highly embedded molecular shocked gas component is an accretion shock in a circumstellar disk. The presentation of the ISO data on the CO, H_2O and OH emission line spectrum of T Tau is left to another paper (Spinoglio et al. 1999). We anticipate that the analysis of these data shows that the physical picture outlined here is confirmed.

2. Observations

An ISO Short Wavelength (2.4–45 μm) Spectrometer (SWS; de Graauw et al. 1996) full grating scan ("AOT S01", speed 4) of T Tau was obtained in ISO revolution 680 (JD 2450717.411). In addition to this, deeper SWS grating scans on selected molecular and fine structure lines ("AOT S02") were obtained in revolutions 681 and 861 (at JD 2450718.778 and 2450897.973). Besides the SWS results, we present here the results of a relatively fast ISO Long Wavelength (43–197 μm) Spectrometer (LWS; Clegg et al. 1996) full grating scan ("AOT L01", t = 776 s) obtained in revolution 672 (JD 2450709.675), while a deeper LWS spectrum is presented in Spinoglio et al. (1999). In this latter work, LWS off-source measurements on positions 80″ to the North, South, East and West of T Tau were also made, whose results we anticipate here. They show that the [C II] 157.7 μm line was the only one detected in the off-source positions.

Data were reduced in a standard fashion using calibration files corresponding to ISO off-line processing software (OLP) version 7.0, after which they were corrected for remaining fringing and glitches. To increase the S/N in the final spectra, the detectors were aligned and statistical outliers were removed, after which the spectra were rebinned to a lower spectral resolution. Fig. 1 shows the resulting ISO spectra. Accuracies of the absolute flux calibration in the SWS spectra range from 7% in the short-wavelength (< 4.10 μm) part to $\approx 30\%$ in the long wavelength (> 29 μm) part (Leech et al. 1997). The LWS absolute flux calibration is expected to be accurate at the 7% level (Trams et al. 1997). Plots of all detected lines, rebinned to a resolution $\lambda/\Delta\lambda$ of 2000 with an oversampling factor of four (SWS), or with the data averaged (LWS), are presented in Fig. 2. Line fluxes for detected lines and upper limits (total flux for line with peak flux 3σ) for the most significant undetected lines on

Table 1. Observed and extinction-corrected (A_V = 1.$^{\rm m}$39) line fluxes and model predictions (in 10^{-16} W m^{-2}) for T Tau.

Line	λ	AOT	Beam	Observed		Model		
	[μm]		[10^{-8} sr]	Measured	Ext. corr.	J-Shock	C-Shock	Total
H_2 0–0 S(0)	28.2188	S02	1.64	$<$ 4.67	$<$ 4.74	0.06	0.01	0.07
H_2 0–0 S(1)	17.0348	S02	1.15	1.80±0.59	1.85±0.61	1.50	0.35	1.85
H_2 0–0 S(2)	12.2786	S02	1.15	$<$ 9.68	$<$ 9.99	1.10	0.76	1.86
H_2 0–0 S(3)	9.6649	S02	0.85	6.81±1.95	7.36±2.10	1.94	5.26	7.20
H_2 0–0 S(4)	8.0251	S02	0.85	3.17±1.05	3.25±1.07	0.24	3.38	3.62
H_2 0–0 S(5)	6.9095	S02	0.85	13.58±2.63	13.78±2.67	0.14	13.65	13.79
H_2 0–0 S(6)	6.1086	S02	0.85	$<$ 8.07	$<$ 8.21	0.01	4.55	4.56
H_2 0–0 S(7)	5.5112	S02	0.85	11.03±2.63	11.24±2.68	0.00	10.65	10.65
H_2 0–0 S(8)	5.0531	S02	0.85	$<$ 4.52	$<$ 4.62	0.00	2.22	2.22
H_2 0–0 S(9)	4.6946	S02	0.85	2.87±0.95	2.94±0.97	0.00	3.40	3.40
H_2 0–0 S(10)	4.4099	S02	0.85	$<$ 3.13	$<$ 3.21	0.00	0.48	0.48
H_2 0–0 S(11)	4.1813	S02	0.85	$<$ 4.67	$<$ 4.81	0.00	0.51	0.51
H_2 0–0 S(12)	3.9960	S02	0.85	$<$ 2.84	$<$ 2.93	0.00	0.05	0.05
H_2 1–0 Q(1)	2.4066	S01	0.85	5.96±1.97	6.46±2.13	0.00	10.14	10.14
H_2 1–0 Q(2)	2.4134	S01	0.85	1.96±0.65	2.13±0.70	0.00	3.19	3.19
H_2 1–0 Q(3)	2.4237	S01	0.85	4.52±1.20	4.90±1.30	0.00	8.86	8.86
H_2 1–0 Q(4)	2.4475	S01	0.85	0.59±0.21	0.64±0.22	0.00	2.34	2.34
H_2 1–0 Q(5)	2.4547	S01	0.85	1.44±0.48	1.56±0.51	0.00	4.77	4.77
H_2 1–0 Q(6)	2.4755	S01	0.85	$<$ 2.63	$<$ 2.84	0.00	0.94	0.94
H_2 1–0 O(2)	2.6269	S01	0.85	6.20±1.23	6.64±1.31	0.00	2.29	2.29
H_2 1–0 O(3)	2.8025	S02	0.85	9.39±0.99	9.96±1.05	0.00	8.58	8.58
H_2 1–0 O(4)	3.0039	S02	0.85	1.26±0.42	1.33±0.44	0.00	2.46	2.46
H_2 1–0 O(5)	3.2350	S02	0.85	2.87±0.73	3.00±0.77	0.00	4.99	4.99
H_2 1–0 O(6)	3.5008	S01	0.85	$<$ 2.29	$<$ 2.39	0.00	0.92	0.92
H_2 1–0 O(7)	3.8074	S01	0.85	1.32±0.43	1.36±0.45	0.00	1.28	1.28
H I Huα	12.3719	S01	1.15	$<$ 6.23	$<$ 6.42	0.01	–	–
H I Huβ + H7δ	7.5083	S02	0.85	$<$ 3.29	$<$ 3.34	0.00	–	–
H I Pfα	7.4600	S02	0.85	$<$ 3.63	$<$ 3.69	0.03	–	–
H I Pfβ	4.6539	S02	0.85	$<$ 4.90	$<$ 5.03	0.02	–	–
H I Brα	4.0523	S02	0.85	10.97±3.00	11.31±3.09	0.10	–	–
H I Brβ	2.6259	S02	0.85	9.61±1.41	10.29±1.51	0.06	–	–
[Fe I] ($^5D_4$–$^5D_3$)	24.0424	S02	1.15	$<$ 1.83	$<$ 1.87	0.05	–	–
[Fe I] ($^5D_3$–$^5D_2$)	34.7135	S02	2.01	$<$ 1.04	$<$ 1.05	0.02	–	–
[Fe II] ($^4F_{9/2}$–$^4F_{7/2}$)	17.9363	S02	1.15	0.52±0.17	0.53±0.18	0.97	0.00	0.97
[Fe II] ($^6D_{9/2}$–$^6D_{7/2}$)	25.9882	S02	1.15	1.85±0.61	1.88±0.62	3.37	0.00	3.37
[Fe II] ($^6D_{7/2}$–$^6D_{5/2}$)	35.3491	S02	2.01	4.23±1.40	4.28±1.41	1.21	0.00	1.21
[Ni II] ($^2D_{5/2}$–$^2D_{3/2}$)	6.6360	S01	0.85	$<$ 8.15	$<$ 8.27	5.86	0.00	5.86
[Ar II] ($^2P_{3/2}$–$^2P_{1/2}$)	6.9853	S01	0.85	9.38±1.72	9.51±1.75	–	0.00	–
[Ne II] ($^2P_{3/2}$–$^2P_{1/2}$)	12.8135	S01	1.15	28.14±7.15	28.88±7.34	29.36	0.00	29.36
[S I] ($^3P_2$–$^3P_1$)	25.2490	S02	1.15	4.09±1.28	4.16±1.30	2.99	0.31	3.30
[Si II] ($^2P_{1/2}$–$^2P_{3/2}$)	34.8152	S02	2.01	12.59±4.16	12.72±4.20	11.69	0.00	11.69
[O I] ($^3P_2$–$^3P_1$)	63.1850	L01	16.3	230.6±16.1	231.5±16.2	233.2	0.80	234.0
[O I] ($^3P_1$–$^3P_0$)	145.535	L01	8.82	$<$ 14.9	$<$ 14.9	5.00	0.05	5.05
[C II] ($^2P_{1/2}$–$^2P_{3/2}$)	157.741	L01	11.6	10.60±0.74	10.61±0.74	5.22	0.00	5.22

Model parameters:

Component	n [cm^{-3}]	v_s [km s^{-1}]	Ω [10^{-8} sr]
J-shock	5×10^4	100	0.03
C-shock	$\approx 10^5$	35	$\approx$ 0.16

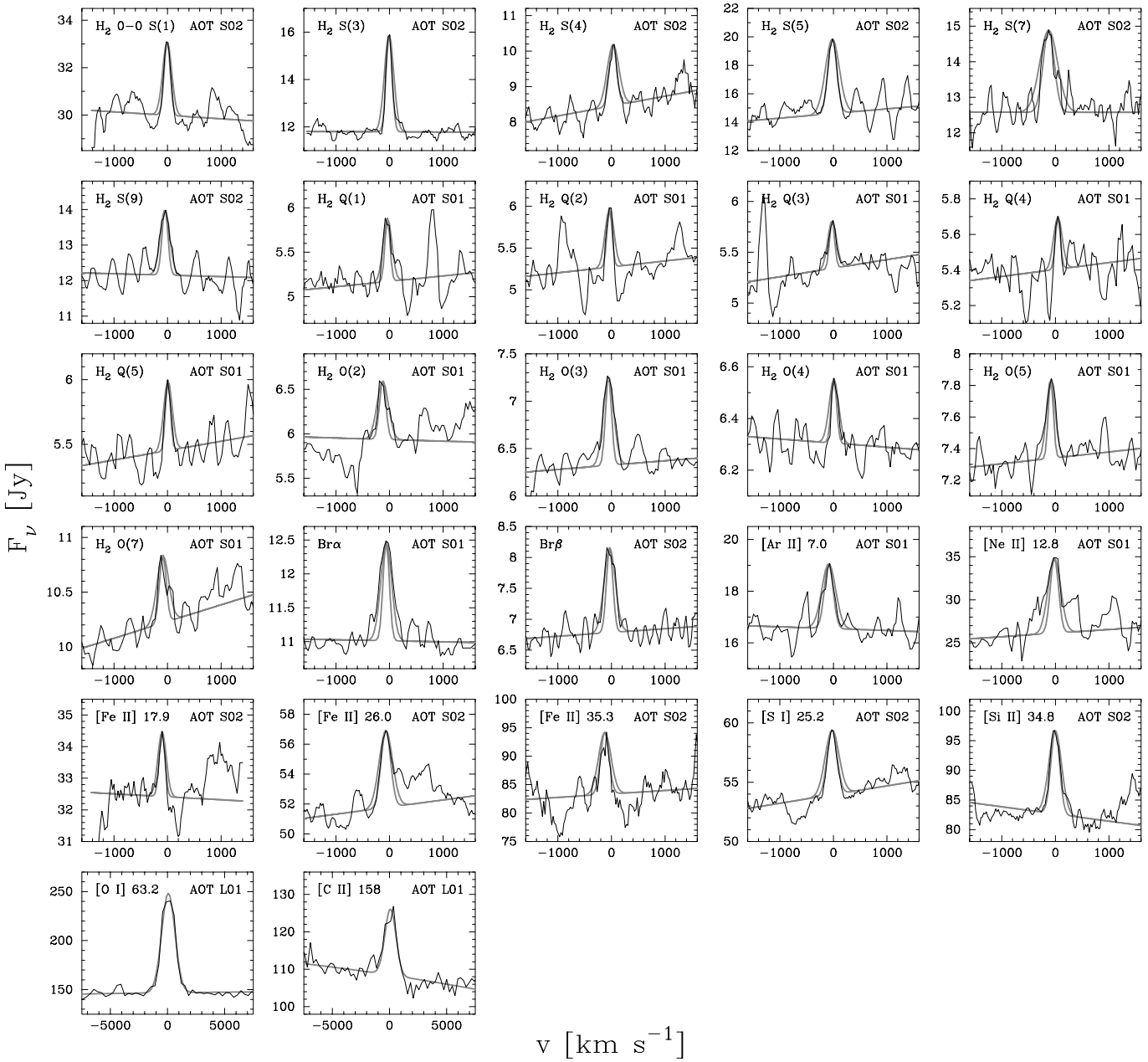

Fig. 2. Detected lines in T Tau. The velocities are heliocentric. The grey lines indicate the instrumental profiles for a point source and an extended source filling the entire aperture.

the on-source position are listed in Table 1. Detected lines in the off-source LWS spectra are listed in Table 2.

For each complete spectral scan, the SWS actually makes twelve different grating scans, each covering a small wavelength region ("SWS band"), and with its own optical path. They are joined to form one single spectrum (Fig. 1). Because of the variation of the diffraction limit of the telescope with wavelength, different SWS bands use apertures of different sizes. For a source that is not point-like, one may therefore see a discontinuity in flux at the wavelengths where such a change in aperture occurs. This effect is not seen in the spectra of T Tau, indicating that the bulk of the infrared continuum comes from a region that is small compared to the smallest SWS beam ($14'' \times 20''$). Note that the same does not have to apply to the line emission.

In the course of this paper we will compare our ISO data of T Tau with measurements by previous authors. To do so accurately, we need to know the relative sizes and orientations of the beams used. Therefore we created a plot of the ISO SWS apertures and LWS average beam size overlaid on a K′-band of the T Tau region (Hodapp 1994), shown in Fig. 3. As can be seen from this figure, all SWS apertures include both T Tau N and T Tau S. They do not include Hind's nebula. The LWS beam includes both the central objects of the T Tauri system as well as Hind's nebula. The fact that the fluxes measured by SWS

Table 2. Line fluxes (in 10^{-16} W m^{-2}) for off-source measurements.

Pos.	α (2000.0)	δ (2000.0)	AOT	λ [μm]	Line	Flux
Off-N	04 21 59.4	+19 33 46.5	L01	157.80	[C II]	7.9±0.9
Off-S	04 21 59.3	+19 20 26.5	L01	157.79	[C II]	8.8±1.3
Off-W	04 22 06.4	+19 32 06.0	L01	157.76	[C II]	8.8±1.1
Off-E	04 21 52.4	+19 32 07.0	L01	157.74	[C II]	9.1±0.9

Table 3. Solid state absorption column densities for T Tau S.

Species	Wavelength [μm]	A_m [cm molec^{-1}]	$\int \tau(\nu)d\nu$ [cm^{-1}]	N [cm^{-2}]
H_2O	3.0	2.0×10^{-16}	109	5.4×10^{17}
H_2O	6.0	1.2×10^{-17}	< 10	$< 8 \times 10^{17}$
CO	4.67	1.1×10^{-17}	< 5	$< 5 \times 10^{17}$
CO_2	4.26	7.6×10^{-17}	12.2	1.6×10^{17}
CO_2	15.2	1.1×10^{-17}	1.2	1.1×10^{17}
CH_4	7.67	7.3×10^{-18}	< 4	$< 5 \times 10^{17}$
Silicate	9.7	1.2×10^{-16}	218	1.8×10^{18}

agree well with those measured by LWS in the small region of overlap, suggests that Hind's nebula remains much fainter than the central objects at wavelengths at least up to 45 μm.

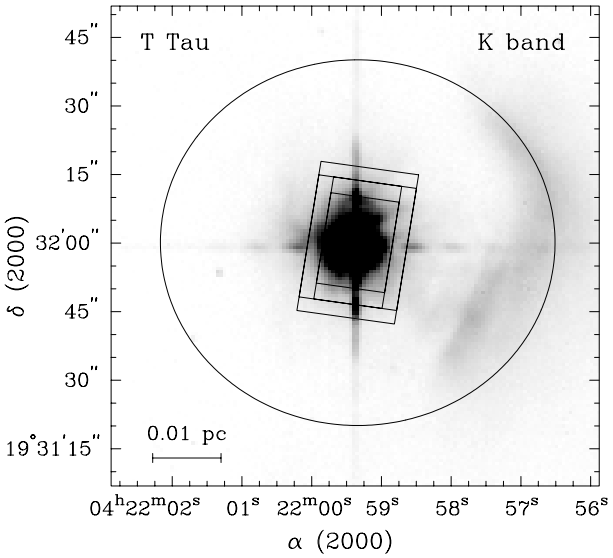

Fig. 3. SWS (rectangles) and LWS (circle; beam FWHM) aperture positions for our measurements of T Tau superimposed on a K′ band image of the region (Hodapp 1994). The orientation of the SWS apertures is nearly identical for the different SWS observations. The rectangles indicate the apertures (in increasing size) for SWS bands 1A–2C (2.4–12.0 μm), 3A–3D (12.0–27.5 μm), 3E (27.5–29.5 μm) and 4 (29.5–40.5 μm).

3. Solid-state features

The SWS spectrum of T Tau (Fig. 1) consists of a smooth continuum with a number of strong absorption features superposed, in which we recognize the O–H bending mode of water ice around 3 μm, the 4.27 μm C=O stretch and the 15.3 μm O=C=O bend of CO_2 and the familiar 9.7 μm absorption feature due to the Si–O stretching mode in amorphous silicates.

By convolving the SWS spectrum with an L band (3.5 μm) transmission curve, we derive a synthetic L magnitude of $3\overset{\mathrm{m}}{.}4$ for T Tau at the time of the observations. This value is within errors identical to the L' band measurement of Simon et al. (1996) in December 1994. Thus the fading of the infrared brightness of the system after the 1990–1991 flare (Ghez et al. 1991; Kobayashi et al. 1994) appears to have ceased before the system has returned to its pre-outburst magnitude. Synthetic 12, 25, 60 and 100 μm fluxes from the ISO spectra are 1.3–1.5 times those measured by IRAS in 1983. The IRAS LRS spectrum is fainter and redder than the ISO SWS spectrum and does not show a 9.7 μm feature in emission or absorption. The ISO SWS fluxes are about 1.4 times less than those in the November 1993 ground-based 8–13 μm spectroscopy by Hanner et al. (1998), in which the silicate feature also appears stronger.

The spectrum obtained with ISO is the sum of the spectra of T Tau N and S. Although T Tau S is expected to dominate the continuum flux in the thermal infrared, T Tau N might also contribute significantly to the spectrum. In particular, absorption features from T Tau S might appear "filled in" with flux from T Tau N, especially in the 9.7 μm silicate feature, which appears in emission in T Tau N, whereas it is in absorption in the southern component (Ghez et al. 1991; van Cleve et al. 1994; Herbst et al. 1997). While the northern component does show variations in brightness in the optical, all available literature data suggest that the infrared variability is limited to T Tau S. We therefore attempt to isolate the contribution from T Tau S (plus the circumbinary envelope at the longer wavelengths) by subtracting an empirical model for T Tau N, consisting of a sum of blackbodies + emission from amorphous silicate at 500 K (Dorschner et al. 1995) fitted to ground-based spatially resolved photometry of T Tau N (Ghez et al. 1991; Herbst et al. 1997), from the data. This model and the resulting spectrum of T Tau S are also shown in Fig. 1. We note that it is possible to reproduce all existing infrared photometry and spectroscopy of T Tau in the literature by the sum of our empirical model of T Tau N and a multiplicative factor times the spectrum of T Tau S. This means that the infrared variations of T Tau S are not caused by variable circumstellar extinction, but must reflect variations in the intrinsic luminosity of the central source, e.g. by variations in the accretion rate.

From the integrated optical depth $\int \tau(\nu)d\nu$ of a non-saturated absorption feature we can compute a column density N using an intrinsic band strength A_m. For H_2O, CO, CO_2 and CH_4 ices, values of A_m were measured by Gerakines et al. (1995) and Boogert et al. (1997). For silicates, A_m is taken from Tielens & Allamandola (1987). Measured integrated optical depth and column densities for T Tau S of commonly observed ices are listed in Table 3. The derived value of 3.4 for the solid H_2O/CO_2 ratio is at the lower range of values observed in the lines of sight towards low-mass YSOs (Whittet et al. 1996; Boogert 1999). Since the line of sight towards T Tau S might actually pass through the outer edge of the T Tau N disk (Hogerheijde et al. 1997), this result may imply that the solid H_2O/CO_2

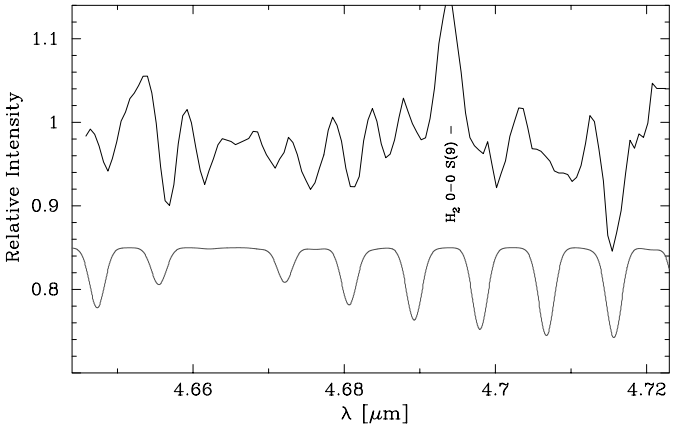

Fig. 4. SWS AOT S02 spectrum of T Tau in the 4.7 μm region, with the continuum normalized to unity (top curve). The peak at 4.694 μm is the 0–0 S(9) transition of molecular hydrogen. Also shown (bottom curve) is a synthetic CO spectrum with $T_{\rm ex}$ = 300 K, b = 5 km s^{-1} and N(CO) = 3 $\times$ 10^{18} cm^{-2}, shifted for clarity.

ratio in the outer disk is similar to those typically found in the envelopes of low-mass YSOs.

Since extinction in the continuum surrounding the 9.7 μm feature is small compared to the extinction within this feature, the extinction A_λ at wavelength λ across a non-saturated 9.7 μm feature can simply be obtained from the relation $A_\lambda = -2.5\log(I/I_0)$. Using an average interstellar extinction law which includes the silicate feature (Fluks et al. 1994), we can then convert these values of A_λ to a visual extinction, resulting in a value of $A_V = 17\overset{\rm m}{.}4 \pm 0\overset{\rm m}{.}6$ toward T Tau S.

4. Gas-phase molecular absorption

Shiba et al. (1993) detected shallow absorption features in the spectrum of T Tau at 1.4 and 1.9 μm, which they identified with warm ($\approx$ 2000 K) water vapour. They argue against a photospheric origin because this would be too hot (K type), and hence locate it in the inner disk. We inspected the ISO SWS spectrum for the presence of absorption from the ν_2 band of gas-phase water, readily seen towards other YSOs (Helmich et al. 1996; van Dishoeck & Helmich 1996; van den Ancker et al. 1999). It is not detected in our T Tau spectra. The resulting upper limit for the H_2O gas-phase column is 10^{18} cm^{-2}, incompatible with the strength of the features observed by Shiba et al. If the dips observed by these authors are indeed real and due to water vapour, they must therefore either be strongly variable, or only occur in the inner disk of T Tau N, which dominates at 1.4 and 1.9 μm.

In the AOT S02 ISO SWS spectrum of T Tau, a number of weak absorption lines with maximum depth around 5% of the continuum level can be seen in the 4.7 μm region (Fig. 4). These could be due to ro-vibrational lines of gas-phase CO. Although weak, some of the lines (especially the 4.717 μm line, which is also present in the AOT S01 spectrum) appear clearly stronger than the noise level. We therefore consider these absorption features as a tentative detection of gas-phase CO in absorption. Following the procedure outlined in van den Ancker et al. (1999), we compared this spectrum with synthetic gas-phase absorption spectra, computed using molecular constants from the HITRAN 96 database (Rothmann et al. 1996). Assuming a Doppler parameter b of 5 km s^{-1} and excitation temperature of 300 K, typical for those observed towards YSOs (Helmich et al. 1996; van Dishoeck & Helmich 1996; Dartois et al. 1998), we derive a total column of CO gas of 10^{18}–10^{19} cm^{-2} for this line of sight.

5. Hydrogen recombination lines

In the ISO SWS spectra of T Tau, the Brα and Brβ lines are present and strong (Table 1). No lines from the higher series of H I were detected. The Brα and Brβ line profiles appear broader than those expected for a point source (Fig. 2). We deduce an intrinsic FWHM of $\approx$ 300 km s^{-1}, in good agreement with the ground-based Brα profile by Persson et al. (1984). The Brα line flux of 11.0×10^{-16} W m^{-2} measured by SWS in a $20'' \times 14''$ aperture is identical to that measured by Evans et al. (1987) in a $3\overset{''}{.}5$ diameter aperture, suggesting that the infrared H I transitions arise in a compact area. Based on the similarity of their Brα line profile to Hα, Persson et al. (1984) suggested that the infrared hydrogen recombination lines from T Tau arise in the optically visible component, T Tau N, and that any H I lines from T Tau S are obscured by many magnitudes of extinction. This is in agreement with spatially resolved images of the T Tau system, in which the Brγ flux is clearly seen to peak at the position of T Tau N (Herbst et al. 1996).

We observe a ratio of the Brα/Brβ line flux of 1.1. Case B recombination line theory can only produce a range of 1.4–2.2 for this ratio (Storey & Hummer 1995). This means that these lines are not optically thin, as assumed in Case B, and that optical depth effects play an important rôle in the radiative transfer. Therefore we can rule out a possible origin in an extended low-density region surrounding T Tau for the H I lines. A similar conclusion was already reached from the Brα/Brγ and Brα/Pfγ lines ratios by Evans et al. (1987). We note that the optical Balmer and Paschen lines follow a similar decrement with increasing quantum number n as the infrared recombination lines. This, together with the similarity of the Brα and Hα profiles noted by Persson et al. (1984) brings us to the conclusion that the optical and infrared H I lines have a similar origin; most likely a stellar wind with a mass loss rate of 3.5 $\times$ 10^{-8} M$_\odot$ yr^{-1} (Kuhi 1964; Kenyon & Hartmann 1995).

For an optically thick ionized wind, Simon et al. (1983) derive a simple relation between Brα line flux and free-free radio emission, which for T Tau predicts a flux of 0.17 mJy at 6 cm. Observed 6 cm radio fluxes of T Tau N are a factor of five higher (Ray et al. 1997). One explanation for this discrepancy could be that we would have underestimated the extinction correction for the Brα line. However, if the optical and infrared H I lines indeed come from the same region, this cannot be the case, since this would render the optical lines invisible. We therefore conclude that only part of the radio flux of T Tau N comes from the wind responsible for the H I lines. An additional source of radio

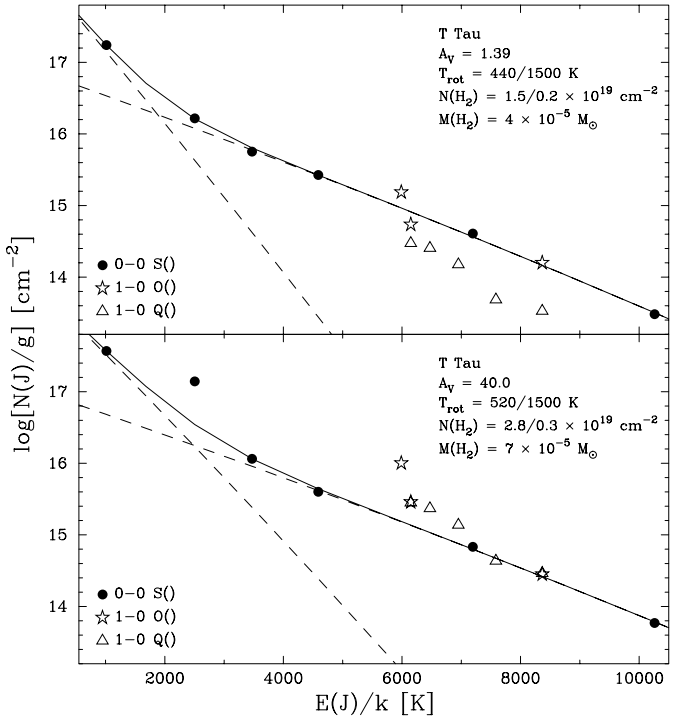

Fig. 5. H_2 excitation diagrams for T Tau, with the data corrected for extinction with A_V = 1.$^{\rm m}$39 (top) and A_V = 40.$^{\rm m}$0 (bottom). For most measurements, formal errors are about the size of the plot symbol. The dashed lines give the Boltzmann distribution fits to the two components of thermal H_2 emission. The solid line shows the sum of both components.

emission must be present in the vicinity of T Tau N, possibly similar to the outflow shock model invoked to explain the non-thermal gyrosynchrotron radio emission from T Tau S (Skinner & Brown 1994; Ray et al. 1997).

6. Molecular hydrogen emission

One property that distinguishes T Tau from other T Tauri stars is the presence of strong UV and near-IR molecular hydrogen emission in its vicinity (Beckwith et al. 1978; Brown et al. 1981). H_2 emission is present throughout Burnham's nebula, but is dominated by emission close to the central binary (van Langevelde et al. 1994b). The source of the central H_2 emission is controversial: Whereas Herbst et al. (1996) claim that both T Tau N and T Tau S contribute about equally to the 1–0 S(1) flux, the adaptive optics images by Quirrenbach & Zinnecker (1997) seem to indicate that most of this bright H_2 emission arises in the vicinity of T Tau S. H_2 emission is also present in a bright knot 2–3″ northwest of the central stars (Herbst et al 1996, 1997) and in less intense knots and filaments throughout the nebula. Previous authors argue that most of the observed H_2 emission must be collisionally excited, in shocks due to the accretion onto T Tau S and the interaction of a collimated outflow with the surrounding medium. However, a fluorescent emission component seems also to be required. The source of the Lyα radiation required for the fluorescence mechanism remains unclear.

Table 4. Extinction determinations from H_2 line flux ratios.

Line ratio	λ_1 [μm]	λ_2 [μm]	$A_{\lambda_1} - A_{\lambda_2}$ [$^{\rm m}$]	A_V [$^{\rm m}$]
1–0 Q(1)/1–0 O(3)	2.4066	2.8025	0.67 ± 0.42	41 ± 26
1–0 Q(2)/1–0 O(4)	2.4134	3.0039	-0.19 ± 0.75	-9 ± 34
1–0 Q(3)/1–0 O(5)	2.4237	3.2350	0.13 ± 0.57	5 ± 22
1–0 Q(4)/1–0 O(6)	2.4475	3.5008	< 3.0	< 97
1–0 Q(5)/1–0 O(7)	2.4547	3.8074	1.34 ± 0.75	39 ± 22

In the SWS spectra of T Tau, we detected pure-rotational (0–0 transitions) emission from H_2 up to S(9) and ro-vibrational (1–0 transitions) lines up to Q(5) and O(7). They are listed in Table 1 and shown in Fig. 2. All lines appear unbroadened at the SWS resolution, showing that they have a small (< 200 km s^{-1}) velocity dispersion and arise in a region much smaller than the beam size. Interestingly, we have detected four pairs of ro-vibrational lines which share the same upper energy level. The ratios of the fluxes for these lines should only depend upon the ratio of the transition probabilities and on extinction. Using the relation $A(\lambda_1) - A(\lambda_2) = 2.5 \log\left(\frac{I_2 \lambda_2 A_{ij,1}}{I_1 \lambda_1 A_{ij,2}}\right)$, with $A(\lambda)$ the extinction at wavelength λ, I the measured line flux and A_{ij} the Einstein A-coefficient, taken from Turner et al. (1977), we can determine the difference in extinction. We then use the extinction law by Fluks et al. (1994) to convert these to a value of A_V. The results of this procedure are listed in Table 4. The 1–0 Q(1)/1–0 O(3) and 1–0 Q(5)/1–0 O(7) line ratios give an extinction of about 40 magnitudes, whereas the 1–0 Q(2)/1–0 O(4) and 1–0 Q(3)/1–0 O(5) line ratios yield much lower values of A_V. Most likely this is because for these ratios the conversion from differential extinction to a value of A_V is erroneous because the 1–0 O(4) and 1–0 O(5) lines are located in the water ice band around 3 microns, prominent in T Tau, which is not included in the Fluks et al. extinction law. However, from the 1–0 Q(3) line flux measured with SWS we compute that a slab of H_2 emitting gas hidden behind the A_V = 40$^{\rm m}$ obtained from the 1–0 Q(1)/1–0 O(3) and 1–0 Q(5)/1–0 O(7) line ratios produces a factor of five less intense 1–0 S(1) radiation than what is observed from the ground. The only way to reconcile these conflicting results is to infer that in fact we are observing ro-vibrational H_2 emission from at least two distinct regions, of which one is heavily embedded ($A_V > 40^{\rm m}$), whereas the other only suffers little extinction. In view of the complex morphology seen in the ground-based 1–0 S(1) images, a scenario with multiple components does not seem unreasonable.

A useful representation of the H_2 data is to plot the log of $N(J)/g$, the apparent column density in a given energy level divided by its statistical weight, versus the energy of the upper level. This plot, in which the data have been corrected for extinction values of A_V = 1.$^{\rm m}$39 and 40.$^{\rm m}$0 and in which high temperature equilibrium relative abundances of 3:1 for the ortho and para forms of H_2 have been assumed, is shown in Fig. 5. For clarity the 1–0 O(4) and O(5) lines, which we were not able to correct for extinction properly, are omitted from this figure. For

a purely thermal population of the energy levels, all apparent column densities should lie on a nearly straight line in Fig. 5. The slope of this line is inversely proportional to the excitation temperature, while the intercept is a measure of the total column density of warm gas. A higher column of H_2 in the lower energy levels of a certain series than predicted by this straight line may be due to fluorescence by Lyα photons (e.g. Black & van Dishoeck 1987; Draine & Bertoldi 1996). Although this effect might also be expected in T Tau, previous observations failed to distinguish this unambiguously from the shocked component. Careful inspection of Fig. 5 shows that in T Tau we have detected two thermal sources of H_2 emission; one responsible for the lines with upper level energy higher than 3000 K and a much cooler component necessary to explain the strong 0–0 S(1) emission. In addition to this, the third component necessary to explain the ground-based near-infrared emission will also contribute to the lines below 3 μm. From Fig. 5 it also becomes immediately evident that the 0–0 S(3) line, at a wavelength within the amorphous silicate band, cannot suffer from great amounts of extinction, provided that the obscuring material contains silicates. The deviation of the apparent column densities of the 1–0 O(2), O(3) and Q(1) lines from the straight line predicted by a purely thermal gas is clear evidence for the presence of the UV fluorescence mechanism.

Following the procedure outlined in van den Ancker et al. (1999) we have fitted a Boltzmann distribution to the two thermal H_2 components, resulting in excitation temperatures of 440 and 1500 K and column densities of 1.5 and 0.2 $\times$ 10^{19} cm^{-2}, respectively. This corresponds to a total H_2 mass of 4×10^{-5} M$_\odot$ or 13 earth masses. The total molecular cloud mass, as derived from CO observations, is several orders of magnitude larger (Momose et al. 1996; Schuster et al. 1997). Therefore we conclude that an additional H_2 source must be present in the T Tau system, whose emission we have failed to detect because its temperature is much lower than the components we have detected here. This component will also contain the bulk of the H_2 mass. Note that this also implies that the bulk of the gas in the CO outflow must be very cool. This is consistent with the 40 K temperature of the outflow derived from ratios of CO line wings by Hogerheijde et al. (1998).

Warm molecular gas can either occur in a photo-dissociation region (PDR) or can be heated by shocks. A shock can either be a J-shock, sufficiently powerful to dissociate molecules, or be a C-shock, which cools mainly through molecular material. Van den Ancker et al. (1998) have employed predictions of H_2 emission from simple, plane parallel PDR, J-shock and C-shock models (Burton et al. 1992; Hollenbach & McKee 1989; Kaufman & Neufeld 1996), to determine the excitation temperature from the low-lying pure rotational levels as a function of density n and either incident far-UV flux G or shock velocity v_s in an identical way as was done for the observations presented here. They arrived at the conclusion that the PDR and J-shock models allow a fairly small (200–540 K) range of excitation temperatures, whereas for C-shocks this range is much larger (100–1500 K). In the model predictions for shocks, $T_{\rm exc}$ does not depend much on density, whereas for PDRs it does not depend much on G. Once the mechanism of the H_2 emission is established, it can therefore be used to constrain v_s or n in a straightforward way.

This means that the 1500 K component can only be caused by a C- (i.e. non-dissociative) shock. From the correlation between excitation temperature and shock speed by van den Ancker et al. (1998), we derive a shock velocity of $\approx$ 35 km s^{-1} for the C-shock. The density and the extent of the shocked gas are poorly constrained. The total column of the 1500 K H_2 component is compatible with either a small ($<$ 5 square arcseconds) region of high ($\approx$ 10^6 cm^{-3}) density, or with a low-density ($\approx$ 10^4 cm^{-3}) region filling a significant fraction ($\approx$ 100 square arcseconds) of the SWS beam. The 440 K H_2 component falls in the parameter space allowed by either J-shock, C-shock and by PDR models. However, the uncertainty in the 440 K temperature is too large to be able to constrain these models any further. Comparison of the absolute line intensities with those predicted by PDR models (Black & van Dishoeck 1987; Draine & Bertoldi 1996) show that the 440 K component can be explained by photon heating if the PDR is located close to the system. These same PDR models are then also able to reproduce the observed UV fluorescence in a natural way. However, shock models can also produce the 440 K component, although current shock models do not include the physics necessary to take into account the UV fluorescence mechanism.

7. Atomic fine structure lines

In the SWS and LWS spectra of T Tau we detected atomic fine-structure lines due to [Fe II], [Ar II], [Ne II], [S I], [Si II], [O I] and [C II]. All lines appear unbroadened at the SWS resolution, suggesting they have a velocity dispersion smaller than 200 km s^{-1} and arise in a region that is compact compared to the beam size. The [O I] 63 μm line was previously detected in T Tau from KAO observations (Cohen et al. 1988). The LWS line flux agrees with that measured by these authors in a 47$''$ aperture. In the LWS spectrum of T Tau, a line is present at the position of [O I] 146 μm, but in view of the strength of other CO lines in the spectrum we attribute most of the line flux to CO J=18–17 and only report an upper limit to the [O I] 146 μm line flux in Table 1. The deeper LWS spectrum of T Tau (Spinoglio et al. 1999) clearly separates the [O I] 146 μm line from the CO J=18–17 emission and a line flux of 8.2 $\times$ 10^{-16} W m^{-2} is derived.

The observed infrared spectrum of T Tau can either originate in a PDR or in one or more shocks. The detection of strong [S I] 25.3 μm emission in T Tau is important, since it is predicted to be weak in PDRs (e.g. Tielens & Hollenbach 1985). It can only reach observable strengths in shock-excited gas. Also, the absence of PAH emission in the SWS spectrum and the non-detection of [O I] emission in the LWS off-source observations argue against a PDR origin of the emission lines. Therefore our working hypothesis will be that the infrared fine structure lines are dominated by shocked gas. Ionized species like [Fe II], [Ne II], [Ar II] and [Si II] which we detected in T Tau cannot be

produced in a C-shock, so we will explain those as arising in a J-shock.

We will try to determine the shock parameters by comparing the line fluxes listed in Table 1 with the J-shock models by Hollenbach & McKee (1989). From their Fig. 7 it can readily be seen that the ratios of the [O I] 63.2 μm, [Fe II] 26.0 μm and [S I] 25.3 μm lines constrain the density well, whereas [Ne II] 12.8 μm is particularly sensitive to shock velocity. A χ^2 fit of line fluxes ratios for T Tau to the Hollenbach & McKee J-shock models yielded a best fit shock velocity $v_s \approx 100$ km s^{-1}, and a density $n \approx 5 \times 10^4$ cm^{-3}. We estimate the errors in these fit parameters to be smaller than 20 km s^{-1} in velocity and smaller than 0.5 dex in density. To reproduce the absolute line fluxes, The J-shock needs to have an extent of 11 square arcseconds. This J-shock will also produce H_2 emission with the strength observed for the 440 K component identified in the previous section. Therefore we infer that this H_2 component is also due to the J-shock.

The line fluxes predicted by the Hollenbach & McKee J-shock models for the best fit parameters are also listed in Table 1. The fit gives satisfactory results, except for the [C II] 157.7 μm, [O I] 145.5 μm, and the [Fe II] lines. The background-corrected [C II] flux of 2.0×10^{-16} W m^{-2} is only half of that predicted by the J-shock model. However, the emergent [C II] flux is strongly dependent on the shock velocity. A model with v_s = 80 km s^{-1} would be able to reproduce the observed fine-structure spectrum, with the exception of [Ne II], which would then appear too strong. Since these differences are within the error with which we think we can determine the shock velocity, we do not consider them significant. The deconvolved [O I] 145.5 μm flux of 8.2×10^{-16} W m^{-2} is 1.6 times that predicted by the J-shock model. However, this line appears stronger than model predictions in many regions where it is observed (e.g. Liseau et al. 1999), so the discrepancy might be caused by a poor knowledge of the atomic data and/or an inadequate understanding of the atomic processes of the oxygen atom. The mismatch of the J-shock model to the [Fe II] fluxes might be more worrisome. The Hollenbach & McKee models predict the 26.0 μm line to be the strongest of the three throughout the parameter space, whereas we observe the 35.3 μm line to be significantly stronger. At present this result lacks a satisfactory explanation.

8. Discussion and conclusions

From the previous sections a complex picture of the T Tau environment emerges. The ISO spectra presented here show evidence for a dusty disk or envelope, an ionized stellar wind, three distinct sources of H_2 emission, and warm atomic gas in dissociative and non-dissociative shocks. What is the origin of all these phenomena? Literature data show that both T Tau N and T Tau S have a circumstellar disk or envelope containing dust and that a dusty circumbinary envelope is present as well. Clearly the continuum data presented here arise in the superposition of these phenomena, with T Tau N dominating at the shortest wavelengths studied here, T Tau S dominant in most of the spectrum, and a contribution of the circumbinary envelope that increases with wavelength. We have seen that the composition of the circumstellar material is by no means unusual: amorphous silicates, water and carbon-dioxide ice and gaseous CO in fairly typical proportions. We derive an extinction of $17\overset{\mathrm{m}}{.}4 \pm 0\overset{\mathrm{m}}{.}6$ in this dust shell. This result resolves the discrepancy between earlier determinations and the $A_V > 7^{\mathrm{m}}$ from the non-detection of T Tau S in HST images (Stapelfeldt et al. 1998). We also found all infrared data to be consistent with a scenario in which T Tau N is constant and T Tau S shows strong wavelength-independent variations in brightness.

The H I data presented in Sect. 5 point to T Tau N as the sole contributing source to these lines. Because our data on these recombination lines extend further to the infrared than previous studies, this does have implications for the mechanism responsible for the radio emission in T Tau S. A scenario in which the continuum radio flux of T Tau S is due to an ionized wind, of which the H I lines are hidden by many magnitudes of extinction is now definitely ruled out by our non-detection of lines from the Pfund and Humphreys series. The outflow shock model to produce non-thermal gyrosynchrotron radiation (Skinner & Brown 1994; Ray et al. 1997) seems more likely and may also be responsible for part of the T Tau N radio flux.

We have distinguished three sources of H_2 emission in our ISO spectra: A cool ($\sim$ 440 K) component suffering little extinction, and two warmer ($\approx$ 1500 K) components, of which one suffers little extinction and the other probably is heavily extincted ($A_V > 40^{\mathrm{m}}$). The far-infrared CO, H_2O and OH emission from T Tau discussed by Spinoglio et al. (1999) show evidence for similar cool and warm temperature components (although OH and H_2O appear overabundant), supporting the picture outlined here. In Sects. 6 and 7 we showed that the cool component can be identified with a dissociative shock or PDR, whereas the non-embedded warm component could be due to a non-dissociative shock. In studying the infrared images by Herbst et al. (1996) we note that the dominant region of [Fe II] 1.64 μm emission is around the H_2 knot T Tau NW. The size of this region is only slightly smaller than the size of 11 square arcseconds required by our J-shock. Therefore we identify T Tau NW as a J-shock in the outflow from T Tau S. Most likely it is a knot in a non-steady outflow, similar to Herbig-Haro objects. The remainder of the shocked ionized emission probably arises from the fainter H_2/[Fe II] knot T Tau SE, which could be a similar knot in the other lobe of the same outflow. The low velocities of these components measured in CO, as well as the morphology and the kinematics of the optical forbidden emission lines suggest that is has an orientation nearly perpendicular ($i \approx 79°$; Solf & Böhm 1999) to our line of sight. It could also drive the giant Herbig-Haro outflow HH 355 (Reipurth et al. 1997).

The location of the C-shock is less clear. Both the "diffuse" and the "west jet" component distinguished by Herbst et al. (1996) have an extent that could produce the required beam filling factor. By comparing the ground-based H_2 imaging results (Herbst et al. 1996; van Langevelde et al. 1994b; Quirrenbach & Zinnecker 1997) with the CO maps of the region by Momose et al. (1996), we note that the "diffuse" component can very well be due to the low-velocity outflow with small ($\approx 10°$) in-

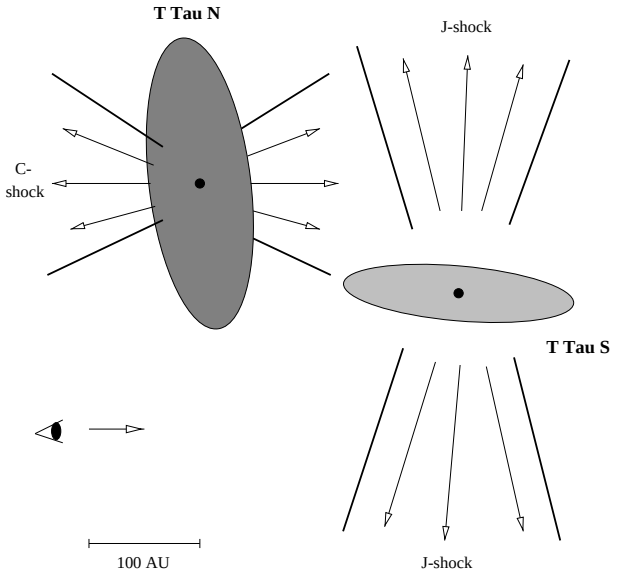

Fig. 6. Schematic picture of the T Tau system with probable sources of C-shock (H_2, [S I]) and J-shock (H_2, [S I], [O I], [Fe II], [Ar II], [Ne II], [Si II], [C II]) emission indicated.

clination angle, presumably arising in T Tau N. Such an outflow could easily produce a C-shock with a large beam filling factor. Therefore we tentatively identify our C-shock with the "diffuse" component, although some contribution from the "west jet" might also be present. A schematic picture of the T Tau system in which we have identified the most likely sources of the detected infrared line emission is shown in Fig. 6.

A remarkable result is the clear signature of the UV fluorescence mechanism in the ro-vibrational H_2 lines. To explain this, an H_2 containing area that is seeing a fairly high number of Lyα photons needs to be present in the T Tau system. However, the low [C II] flux indicate that this area seems to be heated to lower temperatures than predicted by standard PDR models (e.g. Tielens & Hollenbach 1985). This could for example be due to a depletion of small dust particles in the area, consistent with the absence of PAH emission in the SWS spectrum.

We have also found indications for the presence of H_2 emission from a warm, embedded source. In the T Tauri system, only T Tau S suffers significant amounts of extinction, possibly because the line of sight towards T Tau S might pass through the outer edge of the T Tau N disk. Therefore it seems likely that this H_2 component comes from a region in the envelope or disk of T Tau S. An interesting possibility is that we are picking up emission from the shock caused by the impact of circumstellar matter onto the circumstellar disk of T Tau S. If this picture is correct, future H_2 images in e.g. the 1–0 O(5) line should show a morphology that is more concentrated towards T Tau S than the existing 1–0 S(1) data.

The complex situation in the circumstellar environment of T Tau, with multiple outflows and a multitude of shocks, is reminiscent of the situation in the intermediate-mass young stellar object LkHα 225 (van den Ancker et al. 1999). The infrared emission line spectrum of T Tau is also strikingly similar to that of LkHα 225. Interestingly, both LkHα 225 and T Tau are young binary systems consisting an optically visible and an embedded component. It could therefore very well be that these properties that make the T Tau system so unique are not so much related to the central sources, but more to the interaction of the circumstellar disks and outflows with the accretion of matter through a circumbinary disk or envelope.

Acknowledgements. The authors would like to thank M.R. Hogerheijde for useful discussions on the nature of T Tau. We are also especially grateful to Th. de Graauw for his generous allocation of discretionary time for the ISO-SWS observations presented here. MvdA acknowledges financial support from NWO grant 614.41.003 and through a NWO *Pionier* grant to L.B.F.M. Waters. This research has made use of the Simbad data base, operated at CDS, Strasbourg, France.

References

Akeson R.L., Koerner D.W., Jensen E.L.N., 1998, ApJ 505, 358
Beckwith S., Gatley I., Matthews K., Neugebauer G., 1978, ApJ 223, L41
Black F.H., van Dishoeck. E.F., 1987, ApJ 322, 412
Boogert A.C.A., 1999, Ph.D. Thesis, Groningen University
Boogert A.C.A., Schutte W.A., Helmich F.P., Tielens A.G.G.M., Wooden D.H., 1997, A&A 317, 929
Brown A., Jordan C., Millar T.J., Gondhalekar P., Wilson R., 1981, Nat 290, 34
Burton M.G., Hollenbach D.J., Tielens A.G.G.M., 1992, ApJ 399, 563
Calvet N., Hartmann L., Kenyon S.J., Whitney B.A., 1994, ApJ 434, 330
Clegg P.E., Ade P.A.R., Arman D.C., et al., 1996, A&A 315, L38
Cohen M., Hollenbach D.J., Haas M.R., Erickson E.F., 1988, ApJ 329, 863
Dartois E., d'Hendecourt L., Boulanger F., et al., 1998, A&A 331, 651
de Graauw Th., Haser L.N., Beintema D.A., et al., 1996, A&A 315, L49
Dorschner J., Begemann B., Henning Th., Jäger C., Mutschke H., 1995, A&A 300, 503
Draine B.T., Bertoldi F., 1996, ApJ 468, 269
Dyck H.M., Simon T., Zuckerman B., 1982, ApJ 255, 103
Edwards S., Snell R.L., 1982, ApJ 261, 151
Evans N.J., Levreault R.M., Beckwith S., Skrutskie M., 1987, ApJ 320, 364
Fluks M.A., Plez B., Thé P.S., et al., 1994, A&AS 105, 311
Gerakines P.A., Schutte W.A., Greenberg J.M., van Dishoeck E.F., 1995, A&A 296, 810
Ghez A.M., Neugebauer G., Gorham P.W., et al., 1991, AJ 102, 2066
Ghez A.M., Weinberger A.J., Neugebauer G., Matthews K., McCarthy D.W., 1995, AJ 110, 753
Gorham P.W., Ghez A.M., Haniff C.A., et al., 1992, AJ 103, 953
Hanner M.S., Brooke T.Y., Tokunaga A.T., 1998, ApJ 502, 871
Helmich F.P., van Dishoeck E.F., Black J.H., et al., 1996, A&A 315, L173
Herbst W., Booth J.F., Chugainov P.F., et al., 1986, ApJ 310, L71
Herbst T.M., Beckwith S.V.W., Glindemann A., et al., 1996, AJ 111, 2403
Herbst T.M., Robberto M., Beckwith S.V.W., 1997, AJ 114, 744
Hodapp K.W., 1994, ApJS 94, 615
Hogerheijde M.R., van Langevelde H.J., Mundy L.G., Blake G.A., van Dishoeck E.F., 1997, ApJ 490, L99

Hogerheijde M.R., van Dishoeck E.F., Blake G.A., van Langevelde H.J., 1998, ApJ 502, 315
Hollenbach D.J., McKee C.F., 1989, ApJ 342, 306
Kaufman M.J., Neufeld D.A., 1996, ApJ 456, 611
Kenyon S.J., Dobrzycka D., Hartmann L., 1994, AJ 108, 1872
Kenyon S.J., Hartmann L., 1995, ApJS 101, 117
Kessler M.F., Steinz J.A., Anderegg M.E., et al., 1996, A&A 315, L27
Knapp G.R., Kuiper T.B.H., Knapp S.L., Brown R.L., 1977, ApJ 214, 78
Kobayashi N., Nagata T., Hodapp K.W., Hora J.L., 1994, PASJ 46, L183
Kuhi L.V., 1964, ApJ 140, 1409
Leech K., de Graauw Th., Sidher S., et al., 1997, SWS Instrument Data Users Manual. Issue 3.1, SAI/95-221/Dc
Levreault R.M., 1988, ApJS 67, 283
Liseau R., White G.J., Larsson B., et al., 1999, A&A 344, 342
Maihara T., Kataza H., 1991, A&A 249, 392
Momose M., Ohashi N., Kawabe R., Hayashi M., Nakano T., 1996, ApJ 470, 1001
Nisenson P., Stachnik R.V., Karovska M., Noyes R., 1985, ApJ 297, L17
Persson S.E., Geballe T.R., McGregor P.J., Edwards S., Lonsdale C.J., 1984, ApJ 286, 289
Quirrenbach A., Zinnecker H., 1997, The Messenger 87, 36
Ray T.P., Muxlow T.W.B., Axon D.J., et al., 1997, Nat 385, 415
Reipurth B., Bally J., Devine D., 1997, AJ 114, 2708
Robberto M., Clampin M., Ligori S., et al., 1995, A&A 296, 431
Rothmann L.S., Gamache R.R., Tipping R.H., et al., 1996, J. Quant. Spectr. Radiat. Transfer 48, 469
Schwartz P.R., Simon T., Campbell R., 1986, ApJ 303, 233
Schuster K.F., Harris A.I., Russell A.P.G., 1997, A&A 321, 568
Shiba H., Sato S., Yamashita T., Kobayashi Y., Takami H., 1993, ApJS 89 299
Simon M., Felli M., Cassar L., Fischer J., Massi M., 1983, ApJ 266, 623
Simon M., Longmore A.J., Shure M.A., Smillie A., 1996, ApJ 456, L41
Skinner S.L., Brown A., 1994, AJ 107, 1461
Solf J., Böhm K.H., 1999, ApJ, in press
Spinoglio L., Giannini T., Nisini B., et al., 1999, A&A, submitted
Stapelfeldt K.R., Burrows C.J., Krist J.E., et al., 1998, ApJ 508, 736
Storey P.J., Hummer D.G., 1995, MNRAS 272, 41
Tielens A.G.G.M., Allamandola L.J., 1987, In: Hollenbach D.J., Thronson H.A. Jr. (eds.) Interstellar Processes. Reidel, Dordrecht, p. 397
Tielens A.G.G.M., Hollenbach D.J., 1985, ApJ 291, 722
Trams N., Burgdorf M., Gry C., et al., 1997, ISO-LWS Instrument Data Users Manual. Issue 5.0, SAI/95-219/Dc
Turner J., Kirby-Docken K., Dalgarno A., 1977, ApJS 35, 281
van Cleve J.E., Hayward T.L., Miles J.W., et al., 1994, Ap&SS 212, 239
van den Ancker M.E., Wesselius P.R., Tielens A.G.G.M., Waters L.B.F.M., 1998, In: Waters L.B.F.M., et al. (eds.) ISO's View on Stellar Evolution. Ap&SS 255, 69
van den Ancker M.E., Wesselius P.R., Tielens A.G.G.M., 1999, A&A, to be submitted
van Dishoeck E.F., Helmich F.P., 1996, A&A 315, L177
van Langevelde H.J., van Dishoeck E.F., Blake G.A., 1994a, ApJ 425, L45
van Langevelde H.J., van Dishoeck E.F., van der Werf P.P., Blake G.A., 1994b, A&A 287, L25
Weintraub D.A., Kastner J.H., Zuckerman B., Gatley I., 1992, ApJ 391, 784
Weintraub D.A., Sandell G., Huard T.L., et al., 1999, ApJ 517, 819
Whitney B.A., Hartmann L., 1993, ApJ 402, 605
Whittet D.C.B., Schutte W.A., Tielens A.G.G.M., et al., 1996, A&A 315, L357
Wichmann R., Bastian U., Krautter J., Jankovics I., Ruciński S.M., 1998, MNRAS 301, L43